Histol Histopathol (2026) 41: 493-503

Histology and Histopathology
From Cell Biology to Tissue Engineering

ORIGINAL ARTICLE Open Access

Cardiomyoprotective effect of Tanshinone IIA in diabetic cardiomyopathy achieved through enhancing PINK1-Parkin dependent mitophagy

Ke Wu[1,2], Chao Yu[3], Ping Li[4] and Nannan Li[2,5]

[1]Department of Cardiovascular Medicine, [2]Shandong University, Jinan, [3]Department of Pain Medicine, [4]Department of Rehabilitation and [5]Pulmonary and Critical Care Medicine, The Affiliated Tai'an City Central Hospital of Qingdao University, Tai'an, PR China

Summary. This study aimed to explore the beneficial effects and underlying protection mechanism of Tanshinone IIA (TSIIA) in diabetic cardiomyopathy (DCM) from the perspectives of mitophagy and mitochondrial integrity. Here, we found that TSIIA significantly increased STZ-induced body weight (L-TSIIA, 299.5 vs. 276.3; H-TSIIA, 308.3 vs. 276.3) and reduced blood glucose concentration (H-TSIIA, 16.1 vs. 21.5). Meanwhile, TSIIA effectively restored the function and morphology of myocardial tissue in diabetes mellitus (DM) rats. Further, TSIIA has been confirmed to have a protective effect on the ultrastructure and function of myocardial mitochondria, which was achieved through activation of mitophagy, as evidenced by enhanced co-localization of LC3 and COX IV (H-TSIIA, 88188.0 vs. 14829.0). Mechanistically, TSIIA alleviated DCM via activation of the PINK1/Parkin axis, increasing PINK1 (H-TSIIA, 0.5 vs. 0.2), Parkin (H-TSIIA, 0.6 vs. 0.3), Beclin-1 (H-TSIIA, 0.6 vs. 0.2) and LC3II/I (H-TSIIA, 0.5 vs. 0.3) expression, as well as decreasing p62 (H-TSIIA, 1.4 vs. 3.6) expression. This study provided a novel insight into the protective effect of TSIIA in DCM and revealed, for the first time, that TSIIA could noticeably improve STZ-induced DCM by enhancing PINK1-Parkin dependent mitophagy.

Key words: Diabetic cardiomyopathy, Tanshinone IIA, Myocardial function, Mitophagy, PINK1-Parkin

Corresponding Author: Nannan Li, Pulmonary and Critical Care Medicine, The Affiliated Tai'an City Central Hospital of Qingdao University, No. 29 Longtan Road, Tai'an, 271000, Shandong PR China. e-mail: wcqmyg2023@163.com

www.hh.um.es. DOI: 10.14670/HH-18-973

Introduction

Cardiovascular complications remain the leading cause of morbidity and mortality in patients with diabetes mellitus (DM) (Wang et al., 2019). Diabetic cardiomyopathy (DCM) is a DM-induced disease characterized by myocardial fibrosis, left ventricular remodeling, and heart failure, independent of hypertension, coronary artery disease, valvular heart disease, and other known heart diseases (Sun et al., 2021; Cui et al., 2022). According to statistics, the cardiovascular disease risk is approximately 3-4-fold higher in diabetic subjects than that of normal controls (Lu et al., 2023). Despite significant improvements in the management of DM, the incidence and mortality of DCM continue to increase, and the clinical prognosis for patients with DCM remains poor (Yang et al., 2019). Therefore, there is an urgent need to thoroughly elucidate the underlying mechanisms of DCM and develop effective interventions to delay or improve the symptoms of DCM.

Accumulated evidence suggests that the occurrence of DCM may be related to mitochondrial dysfunction, oxidative stress, inflammation, autophagy, renin-angiotensin system activation, calcium processing impairment, and myocardial metabolic abnormalities (Athithan et al., 2019; Paolillo et al., 2019). Although multiple factors may collectively contribute to the development of DCM, the exact mechanisms of this pathological process are poorly understood. Recently, mitochondria have been recognized as the convergence point of several pathologies of diabetes damage, and their dysfunction has been identified as an important cause of DCM (Cai et al., 2022). Damaged mitochondria produce a large amount of reactive oxygen species (ROS), exacerbating mitochondrial damage and leading to a vicious cycle of myocardial cell death. Autophagy is a self-degradative and recycling process that primarily

targets long-lived cytoplasmic proteins (Lekli et al., 2017). There is growing evidence that autophagy is inhibited in the cardiac tissue of type 1 and type 2 DM and contributes to the development of DCM (An et al., 2017; Lekli et al., 2017). Mitophagy is a special type of autophagy that specifically degrades damaged or defective mitochondria and mediates mitochondrial remodeling (Zhou et al., 2023). However, disturbed mitophagy promotes the accumulation of unhealthy mitochondria and the activation of mitochondria-dependent cell death (Bravo-San Pedro et al., 2017). Most reports in the literature show insufficient mitophagy during DCM; conversely, mitophagy activation protects against DCM (Zhang and Ren, 2016; Shao et al., 2020; Yu et al., 2021). The above evidence suggests that controlling mitophagy may provide a novel strategy to restore cardiac function in DCM.

Salvia miltiorrhiza, a well-known traditional Chinese herb, has been widely used in China to treat a variety of diseases (Wu et al., 2023). Tanshinone IIA (TSIIA) is one of the main lipid-soluble pharmacologically active components of *Salvia miltiorrhiza*, and is the most abundant and structurally representative form of Tanshinone, which has been widely studied for its promising pharmacological activity in the treatment and prevention of cardiovascular diseases (Tao et al., 2019). In addition, it has been proven to have potential anti-cancer, anti-oxidant, anti-coagulant, and hypoglycemic effects (Ansari et al., 2021; Fang et al., 2021). Notably, TSIIA has also begun to be used for the treatment of DCM, as it has demonstrated considerable efficacy against DCM. Previous studies have reported that TSIIA can ameliorate diabetic myocardial dysfunction in experimental diabetic rats by inhibiting endoplasmic reticulum stress in cardiomyocytes (Tao et al., 2019; Wu et al., 2023). TSIIA also improves cardiac dysfunction in diabetic rats and inhibits cardiomyocyte apoptosis and mitochondrial biogenic dysfunction (Sun et al., 2011). However, in DCM, limited studies have been conducted on the effect of TSIIA on mitochondrial function, and no studies have reported whether TSIIA can improve DCM through mitophagy, let alone the detailed mechanism. Therefore, in this study, we established a streptozocin (STZ)-induced DCM model to observe the effects of TSIIA on cardiac function and mitochondrial function, and further explore whether TSIIA can improve DCM by affecting mitophagy.

Materials and methods

Animals and groups

A total of 60 six-week-old male Sprague-Dawley rats (160-180 g; Shanghai SLAC Laboratory Animal Co., Ltd., Shanghai, China) were individually housed in separately ventilated cages at a temperature of 22±1°C and humidity of 50±5% with a 12-h light/dark cycle, and were given free access to standard food and water. After one week of adaptive culture, the rats were randomly divided into the following groups: (1) Control group (Control, n=15), (2) Model group (diabetes mellitus, DM, n=15), (3) DM+lower-dose TSIIA group (10 mg/kg, L-TSIIA, n=15), and (4) DM+high-dose TSIIA (25 mg/kg, H-TSIIA, n=15). Rats in groups with TSIIA (T109785, Aladdin, China) were intraperitoneally administered daily at a dose of 10 mg/kg and 25 mg/kg for six weeks, while rats in the control and DM groups were injected with the same volume of vehicle (phosphate-buffered saline, PBS). The experimental procedures were reviewed and approved by the Committee for the Care and Use of Laboratory Animals at the Affiliated Tai'an City Central Hospital of Qingdao University. The study was conducted in accordance with International Laboratory Animal Management Regulations and was reported in accordance with ARRIVE guidelines.

Establishment of a diabetic model

After anesthesia (induction anesthesia was performed with 3% isoflurane, followed by maintenance anesthesia with 2% isoflurane), the rats were subjected to intraperitoneal injection of 60 mg/kg/d STZ in a 10 mM citrate buffer solution (pH 4.5). A one-drop blood sample was obtained two days after STZ injection from all rats through the tip of the tail for the determination of the fasting blood glucose concentration by using a reflectance meter (Accu-Chek, Roche Diagnostics GmbH, Mannheim, Germany). Fasting blood glucose levels over 16 mmol/L were identified as having DM.

Echocardiography

At the end of week 6 following STZ injection, cardiac function was measured by using the Vevo 2100 echocardiography system equipped with a 30 MHz probe (Visualsonics, Toronto, Canada). The following parameters were measured and calculated: left ventricular end diastolic volume (LVEDV), LV posterior wall diameter (LVPWD), interventricular septum diameter (IVSD), LV ejection fraction (EF) and LV fractional shortening (FS).

Hematoxylin and eosin (HE) staining

After sacrifice through exsanguination, myocardial tissue samples were harvested and immediately fixed. Subsequently, they were embedded in paraffin, sectioned, and subjected to standard HE staining to measure histopathological change. Finally, the specimens were observed by fluorescence microscopy (Nikon 80i, Japan).

Transmission electron microscope (TEM)

Following perfusion with 4% paraformaldehyde, the myocardial tissues were dissected and then rinsed in 2.5% glutaraldehyde at 4°C for 4h. The tissues were

rinsed in buffer and post-fixed with 1% osmium tetroxide for 1h at room temperature, dehydrated in graded alcohol (50% ethanol, 70% ethanol, 90% ethanol, 90% acetone, 100% acetone), then transferred to propylene oxide. After embedding and sectioning (60 nm), the samples were double-stained with uranium-lead. Images were acquired by TEM (HT7700, HITACHI) and analyzed using Image-Pro Plus 6.0 software.

Reactive oxygen species (ROS) and adenosine triphosphate (ATP) measurements

Intracellular ROS production was examined using the DHE fluorescent probe. Briefly, the myocardial tissue sections were incubated with the DHE probe for 1h at 37°C in a dark environment. The immunofluorescence images were then photographed. ATP levels in the myocardium were determined according to the instructions of a commercial kit (Beyotime, Shanghai, China). The supernatant of the prepared myocardial tissue was mixed with an equal amount of ATP detection reagent, and then incubated for 5 minutes at room temperature. Then, a series of ATP standards of known concentrations was prepared and processed in the same manner as the samples. The bioluminescence of each standard was measured, and a standard curve was plotted (light intensity vs. ATP concentration). Finally, the ATP concentration was determined in the myocardial sample by comparing its bioluminescence intensity to the standard curve.

Mitochondrial membrane potential

The JC-1 fluorescence staining mitochondrial membrane potential detection kit (Beyotime Institute of Biotechnology) was used to detect changes in mitochondrial membrane potential according to the manufacturer's instructions. Fluorescence intensity was observed under a fluorescence microscope. ImageJ software (National Institutes of Health) was used to analyze the staining intensity value of each group.

Real-time polymerase chain reaction (PCR)

Atrial natriuretic peptide (ANP) and brain natriuretic peptide (BNP) levels were determined by real-time PCR. Briefly, total RNA samples from myocardial tissue were dissolved in TRIzol reagent (Invitrogen, USA). Then, extracted RNA (1 μg) was reverse-transcribed to cDNA using the Transcriptor First Strand cDNA Synthesis kit (Takara Biotechnology Co., Ltd., Tokyo, Japan). The SYBR Green PCR Master Mix Kit (Applied Biosystems USA) was used for the relative quantification of RNA. GAPDH was used as an internal control. The primer sequences were: ANP forward, GGGCTTCTTCCTC TTCCTG and reverse CTGAGACGGGTTGACTTCC; BNP forward, AAGTCCTAGCCAGTCTCCA and reverse GGTCTATCTTCTGCCCAAA; and β-actin forward, GGAGATTACTGCCCTGGCTCCTAGC and reverse GGTCTATCTTCTGCCCAAA.

Immunofluorescence staining

In short, myocardial sections were treated with 4% buffered paraformaldehyde for 20 min and then blocked with 1% BSA and 0.1% Triton-X for 2h at room temperature. Next, the samples were incubated overnight with the desired primary antibodies against light chain 3 (LC3, 1: 100, cat. no. WL01506, Wanleibio), cytochrome c oxidase IV (COX IV, 1: 100, cat. no. 66110-1-Ig, Proteintech), and cleaved caspase-3 (1: 100, cat. no. WL02117, Wanleibio) at 4°C, followed by treatment with a secondary antibody for 1h at room temperature. The immunofluorescence signals were obtained using a fluorescence microscope.

Western blotting

Total protein from rat myocardium tissues was extracted using ice-cold RIPA buffer (Thermo Fisher Scientific, Inc.) and quantified using the bicinchoninic acid (BCA) protein assay (Beyotime, Shanghai, China). Subsequently, prepared protein (30 μg) was separated by 12% SDS-PAGE and transferred to a PVDF membrane. After blocking with 5% non-fat milk for 2h at room temperature, the membranes were incubated overnight at 4°C with primary antibodies of anti-PTEN-induced kinase 1 (PINK1, 1:500, cat. no. WL04963, Wanleibio), anti-Parkin (1:500, cat. no. WL02512, Wanleibio), anti-p62 (1:500, cat. no. WL02385, Wanleibio), anti-LC3B II/I (1:500, cat. no. WL01506, Wanleibio), anti-Beclin-1 (1:500, cat. no. WL02237, Wanleibio), and anti-β-actin (1:1000, cat. no. WL01372, Wanleibio). The following day, blots were incubated with horseradish peroxidase-conjugated secondary antibodies (1:5000; cat. no. WLA023; Wanleibio) for 1h at room temperature. Finally, blotted proteins were detected and quantified using a Gel-Pro-Analyzer.

Statistical analysis

Data were analyzed using GraphPad Prism 5.0. Each experiment was independently repeated three times. Differences between groups were analyzed by One-way ANOVA, followed by Bonferroni's multiple comparisons test. $p<0.05$ was predetermined as statistically significant.

Results

TSIIA significantly reduced blood glucose concentrations and body weight in DM rats

In rats treated with STZ, the blood glucose concentration was significantly increased at two days (19.1 vs. 4.3) and six weeks (21.5 vs. 4.1) in the DM group compared with the Control. TSIIA was beneficial

for reducing blood glucose; the concentration of blood glucose was significantly decreased in the H-TSIIA group (16.1 vs. 21.5) at six weeks when compared with the DM group (Fig. 1A). Compared with rats in the Control group, body weight in the DM (213.3 vs. 220.5), L-TSIIA (217.3 vs. 220.5), and H-TSIIA (218.8 vs. 220.5) groups was decreased two days following STZ injection. Moreover, body weight in the TSIIA groups was significantly increased at six weeks compared with the DM group (L-TSIIA, 299.5 vs. 276.3; H-TSIIA, 308.3 vs. 276.3). However, there were no significant differences between the L-TSIIA and H-TSIIA groups (299.5 vs. 308.3) (Fig. 1B).

TSIIA significantly restored the function and morphology of myocardial tissue in DM rats

Echocardiography was performed six weeks post-TSIIA administration. LVPW (2.1 vs. 1.7), LVEDV (309.9 vs. 238.3), and IVSD (1.9 vs. 1.6) were dramatically increased in the DM group compared with the Control group, while EF (63.2 vs. 83.6) and FS (34.3 vs. 54.3) were sharply decreased, indicating impaired cardiac function. TSIIA (25 mg/kg) treatment markedly improved cardiac function of DM rats, with LVPW (1.8 vs. 2.1), LVEDV (257.9 vs. 309.9), and IVSD (1.7 vs. 1.9) decreased, and EF (75.8 vs. 63.2) and FS increased (45.5 vs. 34.3) (Fig. 2A). Heart weight also decreased significantly after the TSIIA intervention in contrast to

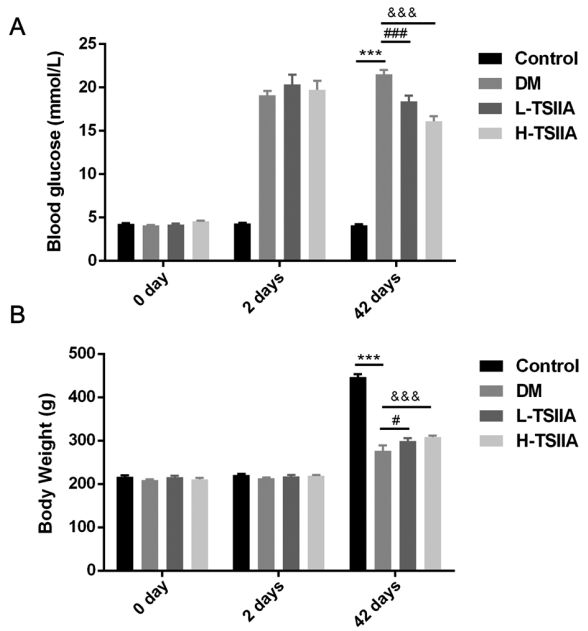

Fig. 1. TSIIA significantly reduced blood glucose concentration and body weight in DM rats. **A.** The blood glucose concentration in each group. **B.** The body weight in each group; ***p<0.001 vs. Control; ###p<0.001 vs. DM; &&&p<0.001 vs. DM; DM, diabetes mellitus; L, lower; H, high; TSIIA, Tanshinone IIA.

DM rats (L-TSIIA vs. DM, 1.1 vs. 1.3; H-TSIIA vs. DM, 1.0 vs. 1.3) (Fig. 2B). HE staining of the myocardial tissue in the DM group indicated clear structural abnormalities, which were characterized by disordered cardiomyocyte arrangement and extensive bleeding, compared with Control animals. Interestingly, TSIIA 25 mg/kg normalized the diabetic morphological changes, and TSIIA 10 mg/kg reduced the number of damaged cardiomyocytes but did not significantly improve the bleeding area (Fig. 2C). By detecting markers associated with heart failure, STZ significantly induced the expression of ANP (4.1 vs. 1.0) and BNP (2.5 vs. 1.0). Treatment with TSIIA25 mg/kg sharply reversed the above gene expression (*ANP*, 1.9 vs. 4.1; *BNP*, 1.6 vs. 2.5), but TSIIA 10 mg/kg only significantly down-regulated the level of *ANP* (2.8 vs. 4.1) (Fig. 2D).

TSIIA protected the mitochondrial ultrastructure and function of myocardial tissue against damage in DM rats

TEM examination revealed that mitochondrial structure was normal in the Control group, with bilayer membranes and cristae present, and myofibrils arranged neatly and consistently. However, the mitochondrial structure of the DM group shrank and became more compact. Furthermore, disordered myofibrils were observed in DM rats. Administration of TSIIA was observed to attenuate the damage induced by STZ. Specifically, it was observed that the mitochondrial structures were recovered and the arrangement of myofibrils was tight (Fig. 3A). Besides, we found that STZ exposure markedly increased mitochondrial ROS production (163331 vs. 5212) and decreased ATP (2.0 vs. 5.1) activity; these changes were alleviated by both L-TSIIA (ROS, 79534 vs. 163331; ATP, 2.8 vs. 2.0) and H-TSIIA (ROS, 32394 vs. 163331; ATP, 4.1 vs. 2.0) treatments (Fig. 3B,C). Correspondingly, TSIIA treatment significantly reduced apoptosis induced by STZ, which can be seen from the reduction in cleaved caspase-3 in both groups (L-TSIIA, 56182 vs. 86439; H-TSIIA, 22495 vs. 86439) (Fig. 4). Energy metabolism abnormalities are likely to impair the structure and function of mitochondria, as indicated by a decrease in $\Delta\psi m$. Our study found that the green fluorescence intensity of the JC-1 monomer, indicating decreased $\Delta\psi m$, increased after STZ stimulation (0.1 vs. 7.9). However, TSIIA increased the red fluorescence intensity, indicating normal membrane potential, especially in the H-TSIIA group (1.8 vs. 0.1) (Fig. 3D,E).

TSIIA significantly enhanced mitophagy in DM rats

Since the clearance of dysfunctional mitochondria can be achieved through mitophagy, we next investigated whether TSIIA mediated mitophagy to remove damaged mitochondria by detecting related markers. LC3 and COX-IV proteins in rat myocardium were labeled with red and green fluorescence, respectively. Here, we found that LC3 and COX-IV

proteins can be co-localized in rat myocardial tissue, indicated by the yellow fluorescence formed by the fusion of red and green. Compared with the Control group, the protein expression of LC3 and COX-IV (14829.0 vs. 120881.0) in myocardial tissue of the DM group was significantly downregulated. Evidently, TSIIA 25 mg/kg administration enhanced autophagic flux, as evidenced by increased LC3 and COX-IV protein expression (88188.0 vs. 14829.0) (Fig. 5).

TSIIA significantly enhanced mitophagy via activation of the PINK1/Parkin axis in DM rats

PINK1/Parkin signaling plays an important role in the development of mitophagy. To further explore the mechanisms underlying TSIIA-enhanced mitophagy, we

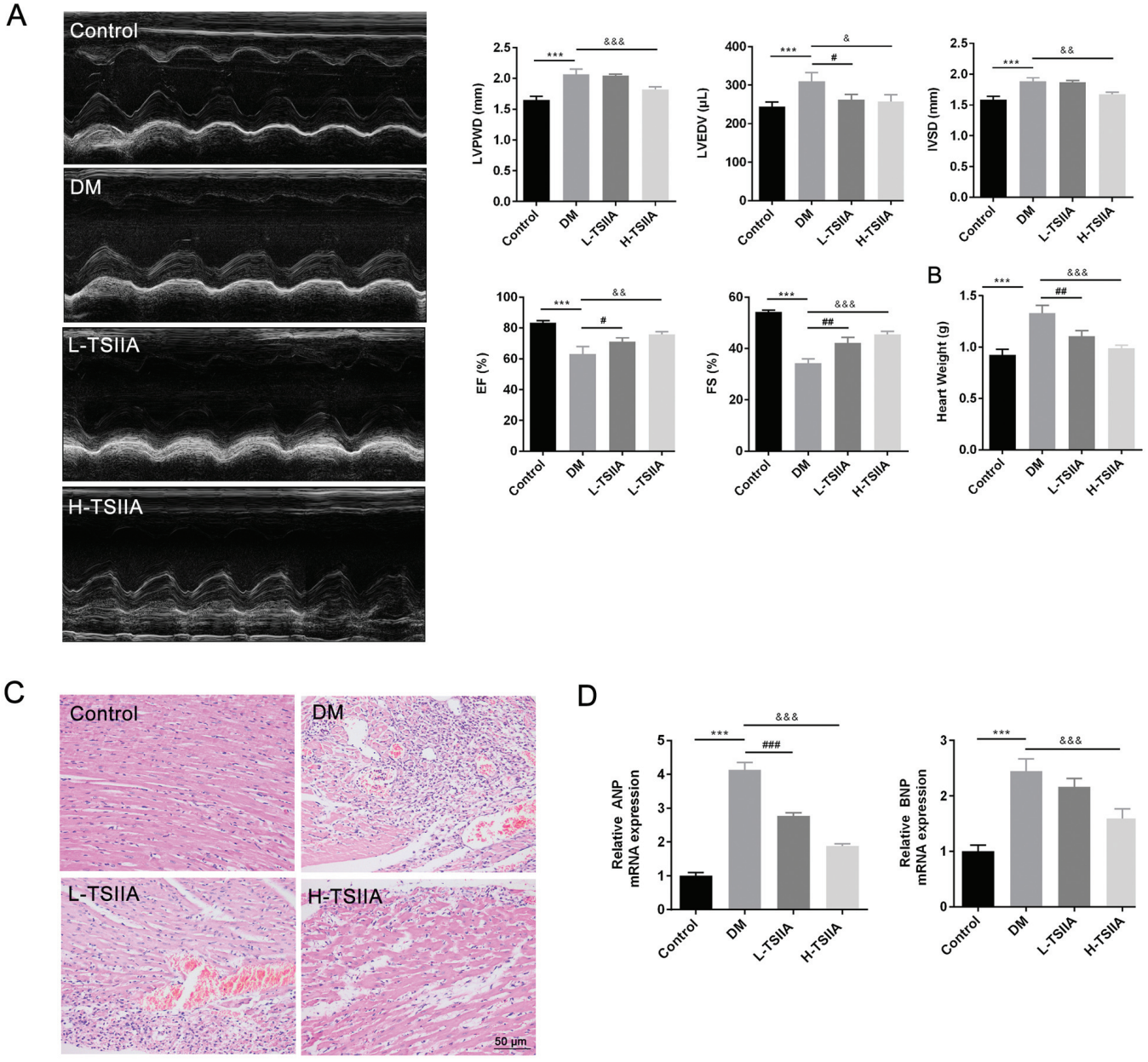

Fig. 2. TSIIA significantly restored the function and morphology of myocardial tissue in DM rats. **A.** Representative echocardiography. **B.** The heart weight in each group. **C.** HE staining of myocardial tissues in in each group. **D.** The detection of ANP and BNP mRNA levels; $^{***}p<0.001$ vs. Control; $^{\#}p<0.5$, $^{\#\#}p<0.01$ vs. DM; $^{\&\&}p<0.01$, $^{\&\&\&}p<0.001$ vs. DM; DM, diabetes mellitus; L, lower; H, high; TSIIA, Tanshinone IIA; ANP, atrial natriuretic peptide; BNP, brain natriuretic peptide.

analyzed related protein expression in the PINK1/Parkin signaling pathway. Not surprisingly, exposure to STZ significantly reduced the protein levels of PINK1 (0.2 vs. 1.0), Parkin (0.3 vs. 1.0), LC3 II/I (0.3 vs. 1.0), and Beclin-1 (0.2 vs. 1.0), while remarkably enhancing p62 (3.6 vs. 1.0) protein levels. TSIIA 25 mg/k significantly reversed protein expression, manifested by the upregulation of PINK1 (0.5 vs. 0.2), Parkin (0.6 vs. 0.3), LC3 II/I (0.5 vs. 0.3), and Beclin-1 (0.6 vs. 0.2), and downregulation of p62 (1.4 vs. 3.6) (Fig. 6).

Discussion

This study provided new evidence to the limited research available on the effect of TSIIA on mitochondrial function. Our findings not only confirmed, for the first time, that TSIIA can improve DCM through mitochondrial autophagy, but also indicated that this benefit depends on the PINK1-Parkin pathway. This research was expected to provide a new paradigm for the modernization of traditional Chinese medicine and promote the recognition and application of traditional Chinese medicine in the international medical field.

Long-term diabetes gradually destroys the cardiac structure, reduces cardiac function, and eventually leads to heart failure, which is one of the main causes of death in diabetic patients (Jia et al., 2018). STZ is a highly selective islet beta-cell cytotoxic drug that interferes with glucose transport, affects the function of glucokinase, destroys islet beta cells, and leads to insufficient insulin secretion (Baig and Panchal, 2019). In our study, the dosage of STZ was sufficient to destroy most islet beta cells and significantly raise blood glucose, while TSIIA significantly reduced blood glucose levels. In addition, we observed that high glucose induced cardiac dysfunction, characterized by significant increases in LVPW, LVEDV, and IVSD, as well as significant decreases in EF and FS. Meanwhile, DM group rats showed significant structural abnormalities. Further evidence emerged from markers associated with heart failure that STZ induced high expression of ANP and BNP. Higher levels of ANP and BNP predict a higher risk of and more severe heart failure (Kuwahara, 2021). As expected, the cardiac function of the rats improved significantly after intervention with TSIIA, which is consistent with the study by Sun et al. (2011).

A previous study has reported that the stress of diabetes represses the oxidative defense mechanism,

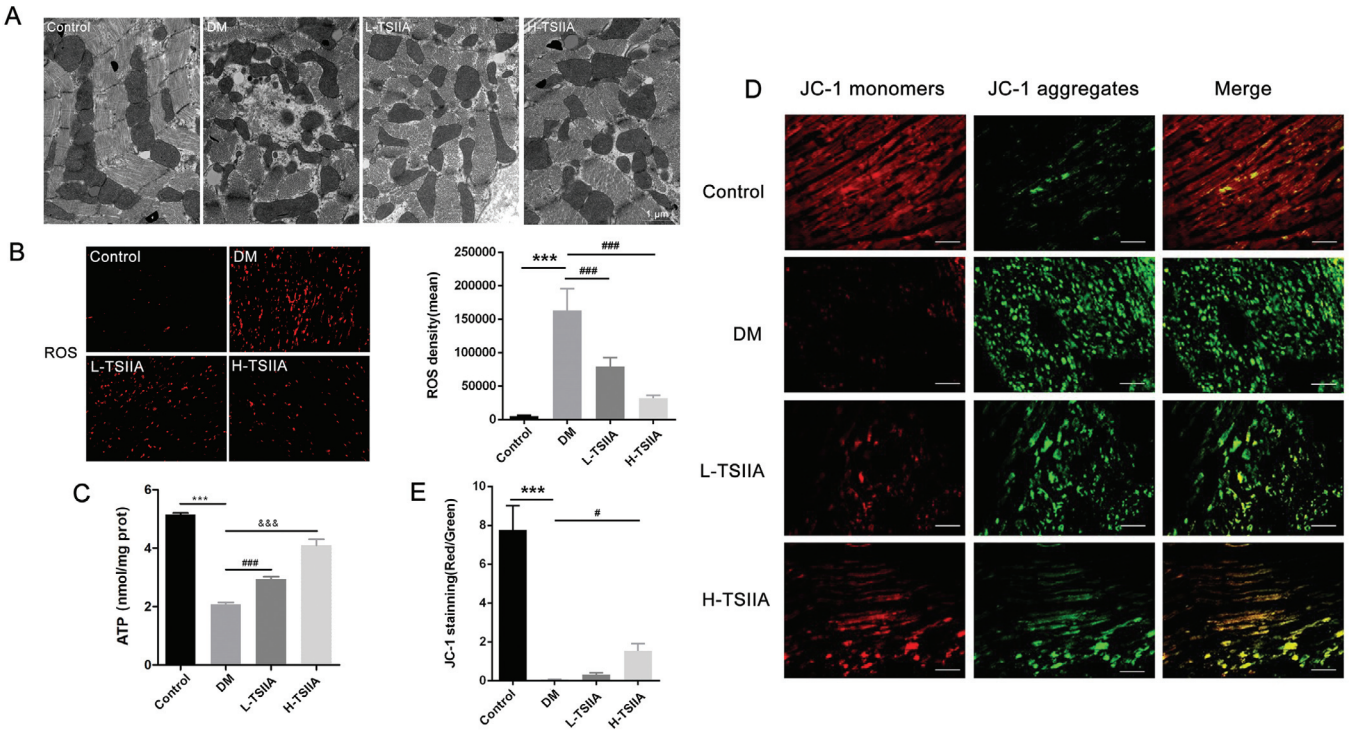

Fig. 3. TSIIA protected the mitochondrial ultrastructure and function of myocardial tissue against damage in DM rats. **A.** Mitochondrial structure in each group. **B.** Intracellular ROS production was examined using a DHE fluorescent probe. **C.** ATP levels in the myocardium were determined via a commercial kit. Determination of the ATP concentration in the myocardial sample by comparing its bioluminescence intensity to the standard curve. **D.** A JC-1 fluorescence staining mitochondrial membrane potential detection kit was used to detect changes in mitochondrial membrane potential. **E.** Quantitative analysis of JC-1 fluorescence staining; ***p<0.001 vs. Control; ###p<0.001 vs. DM; &&&p<0.001 vs. DM; DM, diabetes mellitus; L, lower; H, high; TSIIA, Tanshinone IIA; ROS, reactive oxygen species. B, x 200; D, x 400..

leading to cell destruction, mitochondrial degradation, and possibly inducing DCM six weeks later (Tao et al., 2019). Consistent with these findings, in the present study, mitochondrial ridge loss was observed in DM rats, along with decreased mitochondrial density. However, by applying TSIIA, we found that mitochondrial cristae were partially restored, and mitochondrial density was rescued. A previous study also reported that mitochondrial structure plays a vital role in cardiac function. The degradation of the mitochondrial structure leads to a gradual increase in mitochondrial Ca^{2+} sequestration and depolarization, ultimately leading to cardiac dysfunction (Kyrychenko et al., 2015). The mitochondrial oxidative metabolism provides energy to the myocardium. It makes up 35-40% of the cytoplasm volume and provides 95% of the ATP for the beating adult heart (Wang et al., 2019). In this study, we noted that STZ caused a sharp decrease in ATP in the myocardium, but returned to normal after intervention with TSIIA. ROS accumulation and oxidative stress are key factors in the occurrence and development of diabetic complications, and are also the most prominent initiation signals in the pathological cascade of the diabetic vascular system (Song et al., 2021). Our study found that STZ significantly increased ROS levels in the myocardium of DCM rats, while TSIIA treatment significantly downregulated intracellular ROS, which may partially explain the protective effect of TSIIA against mitochondrial damage. Intracellular ROS can induce the opening of mitochondrial permeability transition pores, releasing proteins such as cytochrome C within mitochondria, resulting in a decrease in $\Delta\psi m$ and blocking of the electron transport chain (Kaludercic and Di Lisa, 2020). Subsequently, cytochrome C binds to the apoptotic protein Apaf-1 to form an apoptotic body, activates caspase, and eventually triggers apoptosis. Here, $\Delta\psi m$ decreased and cleaved caspase-3 was activated under STZ stimulation. These adverse outcomes were mitigated by TSIIA. These data indicated that TSIIA can improve DCM by regulating mitochondrial morphology and function.

Mitophagy is a highly selective form of autophagy that eliminates aging, damaged, or defective mitochondria. It is a crucial means to maintain mitochondrial homeostasis and cell vitality (Wang et al., 2022). In the process of mitophagy, LC3 is a marker of the autophagy process and mainly participates in the formation of autophagosomes. COX IV is a hetero-

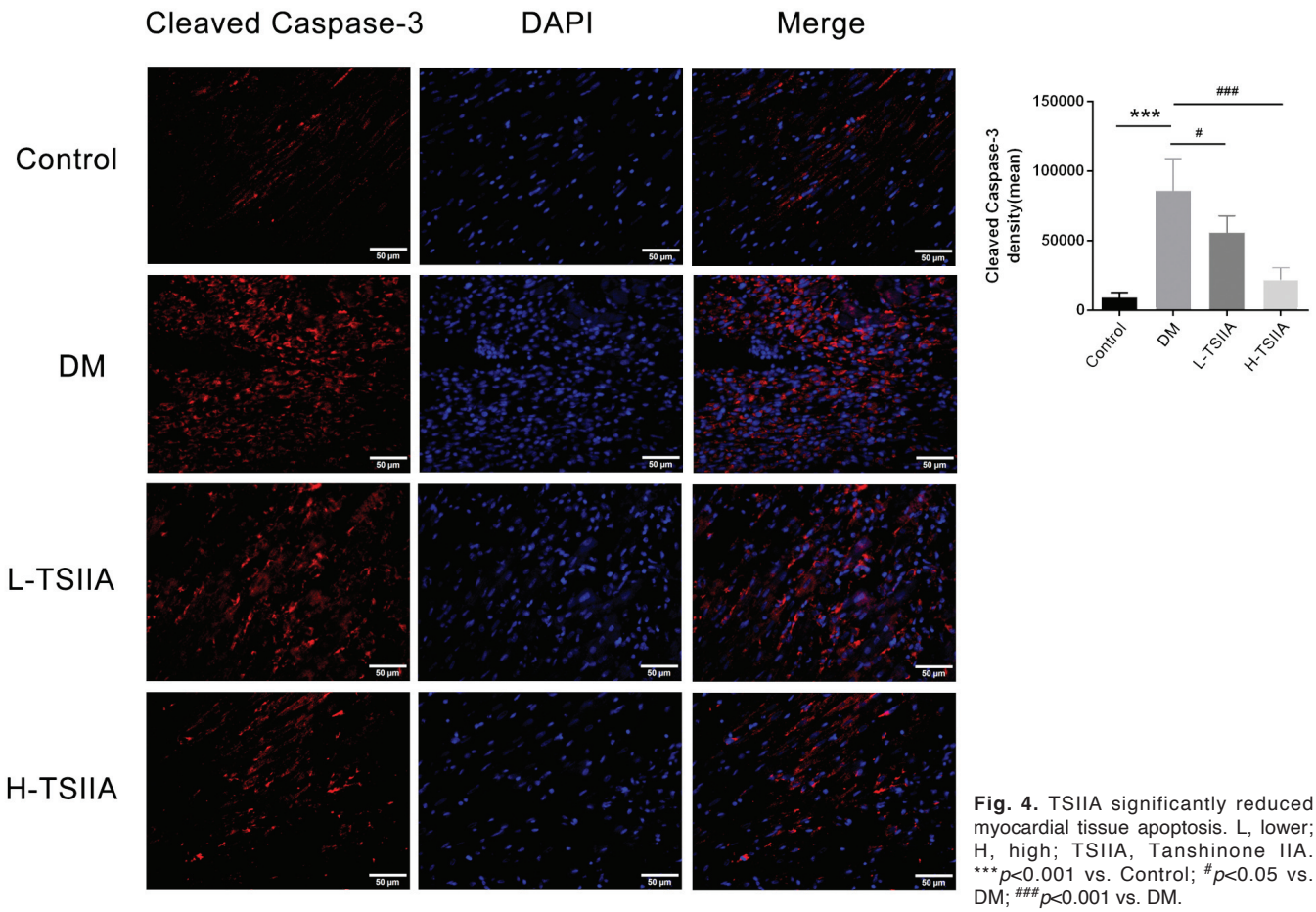

Fig. 4. TSIIA significantly reduced myocardial tissue apoptosis. L, lower; H, high; TSIIA, Tanshinone IIA. ***p<0.001 vs. Control; $^{\#}p$<0.05 vs. DM; $^{\#\#\#}p$<0.001 vs. DM.

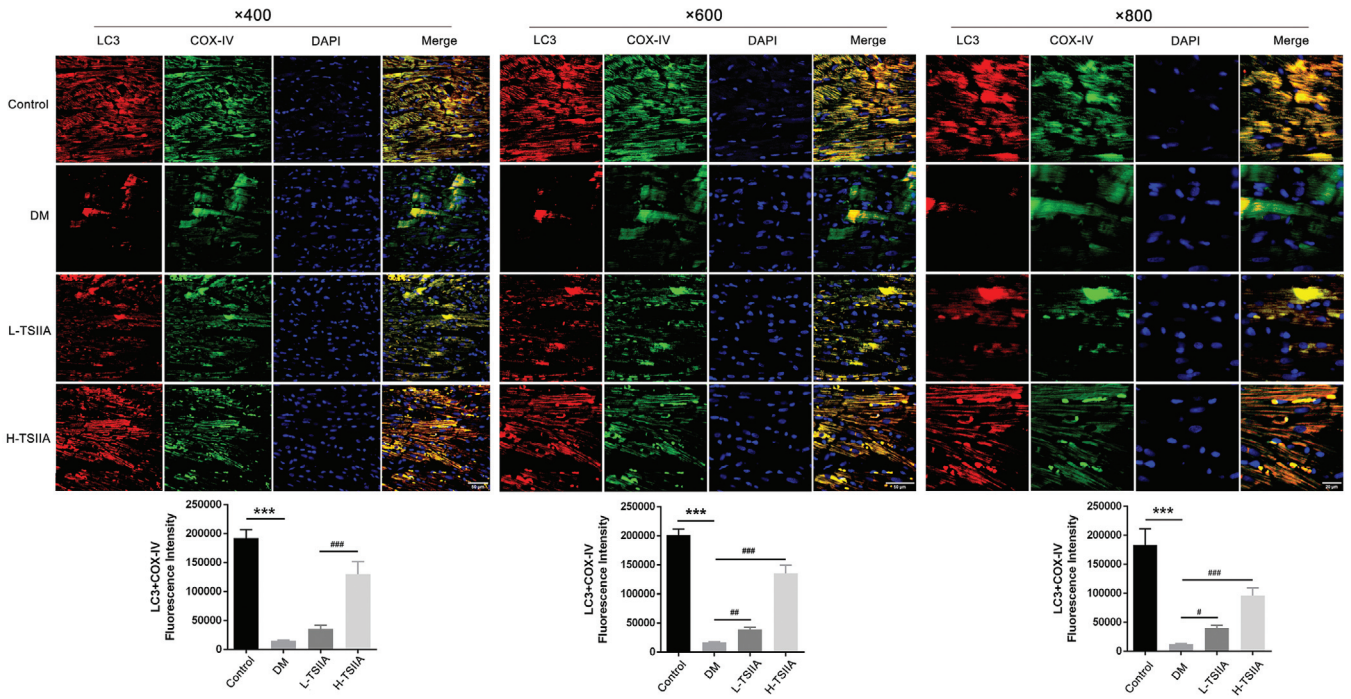

Fig. 5. TSIIA significantly enhanced mitophagy in DM rats. L, lower; H, high; TSIIA, Tanshinone IIA; LC3, light chain 3; COX IV, cytochrome c oxidase IV; Scale, 50 μm. ***p<0.001 vs. Control; ##p<0.01 vs. DM; ###p<0.001 vs. DM.

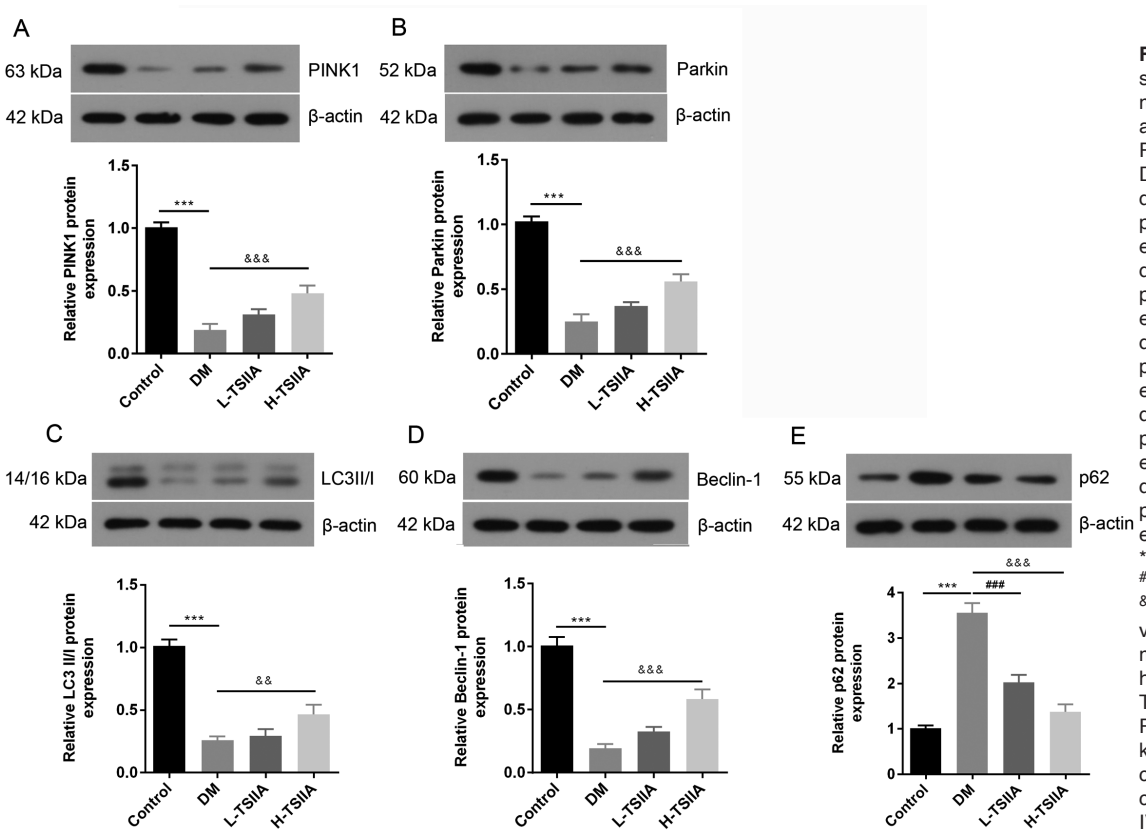

Fig. 6. TSIIA significantly enhanced mitophagy via activation of the PINK1/Parkin axis in DM rats. **A.** The detection of PINK1 protein expression in each group. **B.** The detection of Parkin protein expression in each group. **C.** The detection of LC3II/I protein expression in each group. **D.** The detection of Beclin-1 protein expression in each group. **E.** The detection of p62 protein expression in each group; ***p<0.001 vs. Control; ###p<0.001 vs. DM; &&p<0.01, &&&p<0.001 vs. DM; DM, diabetes mellitus; L, lower; H, high; TSIIA, Tanshinone IIA; PINK1, PTEN-induced kinase 1; LC3, light chain 3; COX IV, cytochrome c oxidase IV.

oligomeric enzyme complex of the mitochondrial respiratory chain, located in the inner mitochondrial membrane (Wei et al., 2021). Available evidence indicates that co-localization of LC3 and COX IV represents ongoing mitophagy (Wang et al., 2023). Liu et al. found that Zhen-Wu-Tang induced mitophagy by increasing the expression of LC3 together with COX IV in the glomerulus to ameliorate renal mitochondrial dysfunction (Liu et al., 2021a). Accordingly, we observed that TSIIA promoted the co-localized expression of LC3 and COX IV in our study, suggesting that TSIIA can alleviate DCM by increasing mitophagy.

The PINK1/Parkin pathway is considered the most important regulatory pathway for controlling mitophagy. Under physiological conditions, PINK1 is primarily processed by the mitochondrial protease PARL when translocated to the mitochondria. When mitochondria are damaged, PINK1 escapes PARL cleavage and accumulates on the outer mitochondrial membrane, where it recruits PRKN and facilitates subsequent ubiquitination. Receptor proteins, including p62, accumulate in the outer membrane of mitochondria, leading to ubiquitination products being recruited into autophagosomes through binding to LC3 and subsequently being degraded (Sekine and Youle, 2018). Liu et al. found that AM1241 exerts a protective effect against MIRI in rats by inducing autophagy through the activation of the Pink1/Parkin pathway, as evidenced by upregulated Pink1, Parkin, Beclin-1, and LC3II/I, as well as downregulated p62 (Liu et al., 2021b). From the data of Mu et al., JQ1 prevents high-fat diet-induced DCM by activating PINK1/Parkin-mediated mitophagy (Mu et al., 2020). As expected, our findings also support the improvement of DCM by PINK1/Parkin-mediated mitophagy. These can be inferred from the increased expression of Pink1, Parkin, Beclin-1, and LC3II/I, as well as decreased expression of p62.

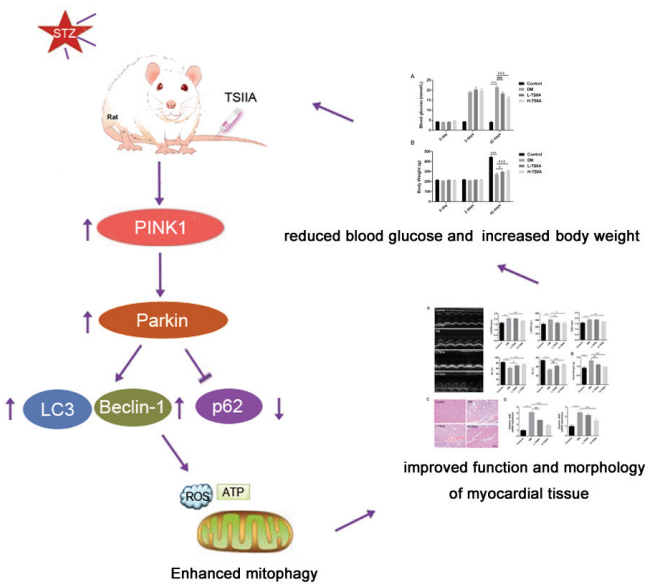

Fig. 7. A schematic diagram depicting the effect of TSIIA on DCM. TSIIA could noticeably improve STZ-induced DCM by enhancing PINK1-Parkin-dependent mitophagy. TSIIA, Tanshinone IIA; STZ, streptozocin; DCM, diabetic cardiomyopathy; PINK1, PTEN-induced kinase 1.

Importantly, we should note that TSIIA reduced blood glucose in DCM rats; however, it still remained at hyperglycemic levels. Oxidative stress caused by a hyperglycemic state may generate ROS through other pathways, such as NADPH oxidase activation, and these ROS may interfere with the initiation and execution of mitophagy. Even though TSIIA can promote mitophagy through the PINK1-Parkin pathway, oxidative stress under hyperglycemic conditions may lead to "false positive" or "false negative" results of mitophagy. Therefore, this may partially counteract the antioxidant effect of TSIIA. What follows might be the restricted regulatory effect on mitochondria and the anti-apoptotic effect of TSIIA. This suggests that we need to further explore the safe dosage at which TSIIA can exert its maximum effect, as well as explore other possible mechanisms. In addition, combination therapy with TSIIA may also be a feasible new strategy for DCM. Undoubtedly, the discovery of new research directions also confirmed the necessity of our study.

Conclusion

Our study revealed, for the first time, that TSIIA could noticeably improve STZ-induced DCM by enhancing PINK1-Parkin dependent mitophagy (Fig. 7). These findings provided novel prospects for TSIIA as a potential therapeutic strategy for DCM. However, it must still be acknowledged that the absence of a TSIIA-only control group remains a methodological limitation. Future studies will further supplement the control group for more in-depth research.

Acknowledgements. Not applicable.

Ethics Statement. The experimental procedures were reviewed and approved by the Committee for the Care and Use of Laboratory Animals at the Affiliated Tai'an City Central Hospital of Qingdao University.

Informed consent. Not applicable.

Consent for publication. All the authors have approved the manuscript.

Data availability statement. The datasets generated during and analyzed during the current study are available from the corresponding author upon reasonable request.

Funding. This study was supported by the Clinical Research Fund of Shandong Medical Association - Qilu Special Project (No. YXH2022ZX02140).

Conflict of Interest. The authors declare that they have no conflict of interest.

Author Contributions. Conception and design: Ke Wu and Nannan Li; Administrative support: Ke Wu; Provision of materials and samples: Ke Wu and Nannan Li; Data collection and collation: Chao Yu, Ping Li; Data analysis and interpretation: Nannan Li and Ping Li.

References

An M., Ryu D.-R., Park J.W., Choi J.H., Park E.-M., Lee K.E., Woo M. and Kim M. (2017). ULK1 prevents cardiac dysfunction in obesity through autophagy-meditated regulation of lipid metabolism. Cardiovasc. Res. 113, 1137-1147.

Ansari M.A., Khan F.B., Safdari H.A., Almatroudi A., Alzohairy M.A., Safdari M., Amirizadeh M., Rehman S., Equbal M.J. and Hoque M. (2021). Prospective therapeutic potential of Tanshinone IIA: An updated overview. Pharmacol. Res. 164, 105364.

Athithan L., Gulsin G.S., McCann G.P. and Levelt E. (2019). Diabetic cardiomyopathy: Pathophysiology, theories and evidence to date. World J. Diabetes 10, 490-510.

Baig M.A. and Panchal S.S. (2019). Streptozotocin-induced diabetes mellitus in neonatal rats: an insight into its applications to induce diabetic complications. Curr. Diabetes Rev. 16, 26-39.

Bravo-San Pedro J.M., Kroemer G. and Galluzzi L. (2017). Autophagy and mitophagy in cardiovascular disease. Circ. Res. 120, 1812-1824.

Cai C., Wu F., He J., Zhang Y., Shi N., Peng X., Ou Q., Li Z., Jiang X., Zhong J. and Tan Y. (2022). Mitochondrial quality control in diabetic cardiomyopathy: From molecular mechanisms to therapeutic strategies. Int. J. Biol. Sci. 18, 5276-5290.

Cui X., Wang J., Zhang Y., Wei J. and Wang Y. (2022). Plin5, a new target in diabetic cardiomyopathy. Oxid. Med. Cell. Longev. 2022, 2122856.

Fang Z.-Y., Zhang M., Liu J.-N., Zhao X., Zhang Y.-Q. and Fang L. (2021). Tanshinone IIA: A review of its anticancer effects. Front. Pharmacol. 11, 611087.

Jia G., Hill M.A. and Sowers J.R. (2018). Diabetic cardiomyopathy: An update of mechanisms contributing to this clinical entity. Circ. Res. 122, 624-638.

Kaludercic N. and Di Lisa F. (2020). Mitochondrial ROS formation in the pathogenesis of diabetic cardiomyopathy. Front. Cardiovasc. Med. 7, 12.

Kuwahara K. (2021). The natriuretic peptide system in heart failure: Diagnostic and therapeutic implications. Pharmacol. Ther. 227, 107863.

Kyrychenko V., Poláková E., Janíček R. and Shirokova N. (2015). Mitochondrial dysfunctions during progression of dystrophic cardiomyopathy. Cell Calcium 58, 186-195.

Lekli I., Haines D.D., Balla G. and Tosaki A. (2017). Autophagy: An adaptive physiological countermeasure to cellular senescence and ischaemia/reperfusion-associated cardiac arrhythmias. J. Cell. Mol. Med. 21, 1058-1072.

Liu B., Cao Y., Wang D., Zhou Y., Zhang P., Wu J., Chen J., Qiu J. and Zhou J. (2021a). Zhen-Wu-Tang induced mitophagy to protect mitochondrial function in chronic glomerulonephritis via PI3K/AKT/mTOR and AMPK pathways. Front. Pharmacol. 12, 777670.

Liu W., Chen C., Gu X., Zhang L., Mao X. and Chen Z. and Tao L. (2021b). AM1241 alleviates myocardial ischemia-reperfusion injury in rats by enhancing Pink1/Parkin-mediated autophagy. Life Sci. 272, 119228.

Lu Q.B., Ding Y., Liu Y., Wang Z.-W., Wu Y.-J., Niu K.-M., Li K.-X., Zhang J.-R. and Sun H.-J. (2023). Metrnl ameliorates diabetic cardiomyopathy via inactivation of cGAS/STING signaling dependent on LKB1/AMPK/ULK1-mediated autophagy. J. Adv. Res. 51, 161-179.

Mu J., Zhang D., Tian Y., Xie Z. and Zou M.H. (2020). BRD4 inhibition by JQ1 prevents high-fat diet-induced diabetic cardiomyopathy by activating PINK1/Parkin-mediated mitophagy in vivo. J. Mol. Cell. Cardiol. 149, 1-14.

Paolillo S., Marisco F., Prastaro M., Renga F., Esposito L., De Martino F., Di Napoli P., Esposito I., Ambrosio A., Ianniruberto M., Mennella R., Paolillo R. and Gargiulo P. (2019). Diabetic cardiomyopathy: Definition, diagnosis, and therapeutic implications. Heart Fail. Clin. 15, 341-347.

Sekine S. and Youle R.J. (2018). PINK1 import regulation; a fine system to convey mitochondrial stress to the cytosol. BMC Biol. 16, 2.

Shao D., Kolwicz S.C. Jr, Wang P., Roe N.D., Villet O., Nishi K., Hsu Y.-W.A., Flint G.V., Caudal A., Wang W., Regnier M. and Tian R. (2020). Increasing fatty acid oxidation prevents high-fat diet-induced cardiomyopathy through regulating parkin-mediated mitophagy. Circulation 142, 983-997.

Song S., Ding Y., Dai G.-L., Zhang Y., Xu M.-T., Shen J.-R., Chen T.-T., Chen Y. and Meng G.-L. (2021). Sirtuin 3 deficiency exacerbates diabetic cardiomyopathy via necroptosis enhancement and NLRP3 activation. Acta Pharmacol. Sin. 42, 230-241.

Sun D., Shen M., Li J., Li W., Zhang Y., Zhao L., Zhang Z., Yuan Y., Wang H. and Cao F. (2011). Cardioprotective effects of tanshinone IIA pretreatment via kinin B2 receptor-Akt-GSK-3β dependent pathway in experimental diabetic cardiomyopathy. Cardiovasc. Diabetol. 10, 4.

Sun H.J., Wu Z.Y., Nie X.W., Wang X.Y. and Bian J.S. (2021). An updated insight into molecular mechanism of hydrogen sulfide in cardiomyopathy and myocardial ischemia/reperfusion injury under diabetes. Front. Pharmacol. 12, 651884.

Tao S., Chen L., Song J., Zhu N., Song X., Shi R., Ge G. and Zhang Y. (2019). Tanshinone IIA ameliorates diabetic cardiomyopathy by inhibiting Grp78 and CHOP expression in STZ-induced diabetes rats. Exp. Ther. Med. 18, 729-734.

Wang S., Zhao Z., Fan Y., Zhang M., Feng X., Lin J., Hu., Cheng Z., Sun C., Liu T., Xiong Z., Yang Z., Wang H. and Sun D. (2019). Mst1 inhibits Sirt3 expression and contributes to diabetic cardiomyopathy through inhibiting Parkin-dependent mitophagy. Biochim. Biophys. Acta Mol. Basis Dis. 1865, 1905-1914.

Wang S., Tan J., Miao Y. and Zhang Q. (2022). Mitochondrial dynamics, mitophagy, and mitochondria-endoplasmic reticulum contact sites crosstalk under hypoxia. Front. Cell Dev. Biol. 10, 848214.

Wang W., Zhang Y., Huang W., Yuan Y., Hong Q., Xie Z., Li L., Chen Y., Li X. and Meng Y. (2023). Alamandine/MrgD axis prevents TGF-β1-mediated fibroblast activation via regulation of aerobic glycolysis and mitophagy. J. Transl. Med. 21, 24.

Wei X., Wu Y.E., Wang W., Zhang S., Liu D. and Liu H. (2021). Decreased dynamin-related protein 1-related mitophagy induces myocardial apoptosis in the aging heart. Acta Biochim. Biophys. Sin. 53, 1354-1366.

Wu S., Lu D., Gajendran B., Hu Q., Zhang J., Wang S., Han M., Xu Y. and Shen X. (2023). Tanshinone IIA ameliorates experimental diabetic cardiomyopathy by inhibiting endoplasmic reticulum stress in cardiomyocytes via SIRT1. Phytother. Res. 37, 3543-3558.

Yang F., Qin Y., Wang Y., Meng S., Xian H., Che H., Lv J., Li Y., Yu Y., Bai Y. and Wang L. (2019). Metformin inhibits the NLRP3 inflammasome via AMPK/mTOR-dependent effects in diabetic cardiomyopathy. Int. J. Biol. Sci. 15, 1010-1019.

Yu L.M., Dong X., Xue X.-D., Xu S., Zhang X., Xu Y.-L., Wang Z.-S.,

Wang Y., Gao H., Liang Y.-X., Yang Y. and Wang H.-S. (2021). Melatonin attenuates diabetic cardiomyopathy and reduces myocardial vulnerability to ischemia-reperfusion injury by improving mitochondrial quality control: Role of SIRT6. J. Pineal Res. 70, e12698.

Zhang Y. and Ren J. (2016). Epigenetics and obesity cardiomyopathy: From pathophysiology to prevention and management. Pharmacol. Ther. 161, 52-66.

Zhou H., Dai Z., Li J., Wang J., Zhu H., Chang X. and Wang Y. (2023). TMBIM6 prevents VDAC1 multimerization and improves mitochondrial quality control to reduce sepsis-related myocardial injury. Metabolism 140, 155383.

Accepted July 29, 2025